Gaussian Attractive Potential for Carboxylate/Cobalt Surface Interactions

Xiaojing Wu,[1] Stephan N. Steinmann,[1] and Carine Michel[1]
École Normale Supérieure de Lyon, CNRS, Laboratoire de Chimie UMR 5182, 46 allée d'Italie, F-69364 Lyon, France.

(*Electronic mail: carine.michel@ens-lyon.fr)

Ligand-decorated metal surfaces play a pivotal role in various areas of chemistry, particularly in selective catalysis. Molecular dynamics simulations at the molecular mechanics level of theory are best adapted to gain complementary insights to experiments regarding the structure and dynamics of such organic films. However, standard force fields tend to capture only weak physisorption interactions. This is inadequate for ligands that are strongly adsorbed such as carboxylates on metal surfaces. To address this limitation, we employ the Gaussian Lennard–Jones (GLJ) potential, which incorporates an attractive Gaussian potential between the surface and ligand atoms. Here, we develop this approach for the interaction between cobalt surfaces and carboxylate ligands. The accuracy of the GLJ approach is validated through the analysis of the interaction of oxygen with two distinct cobalt surfaces. The accuracy of this method reaches a root mean square deviation (RMSD) of about 3 kcal/mol across all probed configurations, which corresponds to a percentage error of roughly 4%. Application of the GLJ force field to the dynamics of the organic layer on these surfaces reveals how the ligand concentration influences the film order, and highlights differing mobility in the x and y directions, attributable to surface corrugation on Co(11$\bar{2}$0). GLJ is versatile, suitable for a broad range of metal/ligand systems, and can, subsequently, be utilized to study the organic film on the adsorption/desorption of reactants and products during a catalytic process.

I. INTRODUCTION

Organic/inorganic interfaces are central to a wide range of domains in both fundamental research and practical applications. Organic lubrication modifiers,[1] functional organic materials in batteries[2] or collector molecules for mineral flotation[3] are examples illustrating the breadth of the practical applications of such interfaces. In fundamental research, understanding bio-mineralization,[4] molecular electronics,[5] engineering nanomaterials with shape-directive agents[6,7] or tuning heterogeneous catalytic sites with ligands[8–10] are all connected to fundamental questions related to the organic/inorganic layers[11,12]. How does the inorganic surface influence the structuring of the organic layer (and vice-versa)? What is the dynamical behavior of the organic layer? Can a small molecules penetrate the organic film to reach the inorganic surface? Insights from molecular modelling are apt to provide answers to these questions, provided a qualitatively correct description of the system is achieved.

Assessing the dynamics of the organic layer is critical when the question of the surface accessibility is key such as in corrosion, catalysis or ligand-exchange reactions. At the organic/inorganic interface, the organic molecules may desorb and diffuse away from the inorganic surface[10,13] but also diffuse more or less easily parallel to the surface plane depending on the surface, concentrations and temperature.[14] This parallel diffusion would be problematic if the organic layer was intended to protect the inorganic surface.[15] However, the diffusion might be essential to let small molecules reach the inorganic surface and when the organic film aims at at tuning the efficiency and selectivity of heterogeneous catalysts.[8–10,16–18]

Characterizing the dynamics of an organic film is highly challenging experimentally, even though bound and free carboxylate ligands can be distinguished using NMR,[19] and model systems can be investigated by scanning tunneling microscopy.[14] In practice, experimental investigations of these films are often interpreted in conjunction with molecular modeling to reach a molecular understanding of the experimentally observed phenomenon.[20] This approach was recently successfully applied to carboxylate ligands on CdSe nanocrystals.[21] It has also been beneficial in understanding the structuring of a liquid when in contact with a surface[22–25], as well as in the study of adsorption at the solid/liquid interface.[26–28] Molecular dynamics (MD) is the work-horse of the field to sample the accessible structures and derive structural and dynamical properties. Energies and forces could, ideally, be computed *ab initio* using density functional theory (DFT). However, these Born-Oppenheimer MD studies face the limitation of their computational cost, which translates into short (below 100 ps) trajectories. This limitation can partially be overcome by enhanced-sampling techniques such as metadynamics[27,29] or thermodynamic integration,[27,30] but the lack of full equilibration of the system remains an often overlooked factor that puts large uncertainties on the obtained results. Moving to molecular mechanics (MM) (i.e., classical force fields) allows a significantly more efficient sampling, reaching the ns range. Forces fields are less developed for organic/inorganic interfaces than for bio-systems, where they are well established.[31] One of the challenges is the diversity of types of atoms and thus of the number of interactions to fit and the other is a general scarcity of reliable, relevant experimental data to constrain the fit. If the interfacial interactions are weak according to ab initio computations, they can be described by the typical combination of a Lennard–Jones potential and electrostatic forces, as, for instance, done by Pensado et al.[22] to study Ru nanoparticles in ionic liquids. An alternative is to adjust the force field parameters, to fit interface-related experimental data as proposed by Heinz and co-workers.[32] However, no parameters are available for cobalt.

To predict the dynamic behavior of relatively strongly bonded organic molecules to metallic surfaces and capture

their binding site preferences requires an original approach: desorption may be very limited while diffusion along the surface may still occur, depending on the diffusion barrier. A possibility could be to derive machine-learning based force fields[8,33–37], but the lack of transferability and the amount of data that is required for those complex systems makes this approach prohibitive. Similarly, reactive force fields (ReaxFF) can be used to describe reactive events at interfaces.[26] However, this also comes with the challenge of demanding system-dependent parameterizations. Inspired by the GolP force field developed by Corni and co-workers[38,39] for peptide adsorption at aqueous/Au interfaces, we have recently proposed the GAL force field to describe water/metal interaction,[40,41] reaching a functional form that can also describe metallic nanoparticles in water.[42] Besides a typical long-range attractive term and a short-range repulsion term, this metal-water force field includes an angular dependence and, most importantly, an attractive Gaussian centered on the surface metal atoms. We then extended this approach to describe the interaction between organic molecules containing oxygen and nitrogen heteroatoms with alumina and hematite surfaces. Augmenting a standard Lennard–Jones potential with an attractive Gaussian was found to lead to an accurate, easily transferable functional form, applicable to various O or N containing molecules. We call this approach GLJ.[43] The advantage of GLJ compared to other approaches is its simplicity: just adding an attractive Gaussian to better describe the near chemisorption of organic molecules onto inorganic surfaces allows to use well-established force-fields for organic molecules for a wide range of organic ligands, while reproducing a reasonable adsorption strength and a qualitatively correct adsorption site preference.

The dynamics of carboxylates on inorganic surfaces is critical to engineer nanomaterials[6,44,45] but also to use them as catalysts.[46–51] We have recently shown that Co nanoparticles that are decorated with various carboxylate ligands are catalytically active towards the alcohol dehydrogenation reaction, producing "green" H_2 and value-added ketones.[46]. Among the tested catalysts, the rod-shaped Co nanoparticles decorated with the laurate ligand ($C_{11}H_{23}COO\cdot$) exhibited the highest catalytic rate.[46] The influence of the morphology was rationalized using periodic DFT models to investigate the catalytic profiles in presence of model carboxylate (acetate). The ability of the ligands to adapt to the reactive events was found to be critical but cannot be easily quantified using DFT models.[46]

The diffusion of the carboxylate films should be better described using classical molecular dynamics than DFT if a reliable force field is available. The active Co nanoparticles majorly expose two types of surface facets, the (0001) and the $(11\bar{2}0)$. The carboxylate ligands are strongly bonded to both facets as demonstrated by successive washings, transmission electron microscopy (TEM) and thermogravimetric analysis (TGA). This strong bonding can be easily related to the oxophilicity of Co and is well-reproduced by DFT computations. It is also well in line with surface science experiments using formic acid as a model carboxylic acid.[52] Even if the ligands cannot easily desorb, they may diffuse parallel to the surface, a process that could be affected by the underlying structure of the metallic facet. Hence, this dynamical property may dictate which facet is the most accessible to a target molecule. However, as a first step, one needs to ensure that the force field captures the relevant physics: adsorption strengths, site preferences and diffusion barriers. Here, we aim at the development of this force field. The use of the force field to gain insights in the catalytic reaction will be reported at a later stage, focusing on the diffusion of reactant and products through the organic layer.

To assess how the in-plane dynamics of an organic layer is tuned by the nature of the underlying inorganic surface, we investigate the Co-carboxylate case by comparing the (0001) and $(11\bar{2}0)$ facets. We first fitted the GLJ Co-carboxylate potential for each facet against state-of-the art DFT calculations. Then we demonstrate that using our original approach based on attractive Gaussians in combination with a typical Lennard–Jones potential leads to contrasted dynamics of the organic film.

II. COMPUTATIONAL DETAILS

A. DFT Computations

All DFT computations were performed with the Vienna Ab initio Simulation Package (VASP 6.2.1)[53,54] using the PBE generalized gradient approximation functional[55] with the dDsC dispersion correction[56,57] and an energy cutoff of 400 eV for the expansion of the plane-wave basis. The electron–core interactions are described by the PAW formalism[58,59]. The SCF convergence criterium was set at 10^{-6} eV. Spin polarization has been accounted for. The initial magnetic moment value for each Co atom was set to 1.63 μB. The Co-Co distance was optimized for the bulk and found to be 2.47 Å, which compares well with the experimental value of 2.51 Å. Two surface were cleaved from the optimized bulk, the (0001) and $(11\bar{2}0)$ with ($p(3\times3)$, 4 layers) and ($p(4\times4)$, 6 layers) respectively. The structure of both slabs is shown in Figure 1. The first layer is highlighted in green, and the corrugation of these two surfaces is quite distinct. On the Co(0001) surface, the *xy* directions are equivalent, whereas the Co$(11\bar{2}0)$ surface exhibits asymmetry, with Co-Co distances measuring 2.47 Å along the *x*-direction and 4.28 Å along the *y*-direction. The slabs are separated by a vacuum of 15 Å in order to minimize interactions between periodic images. The Brillouin zone was sampled by a Γ-centered $3\times3\times1$ Monkhorst-Pack *k*-point grid. A series of 198 configurations were built of a single acetyloxyl radical molecule ($CH_3CO_2\cdot$) adsorbed on each facet. The geometry of the acetyloxyl radical molecule was taken from DFT optimizations on each surface, with the slab frozen (C-O 1.28 Å, O-C-O 124.2° and 123.8° on Co(0001)and Co(11-20) surfaces, respectively). Starting from the optimized configuration, the adsorbate was rotated around the *z*-axis by fixing one oxygen atom, scanning three values for the angle (ω). The rotated structures are translated by eleven different distances (d) to explore possible adsorption sites (see Figure S1). Similarly, six different distances from

the surface (z) were chosen to evaluate the out-of-plane dependence of the adsorption energy at all probed locations. To further assess the quality of the fit, a test set of 20 structures have been generated according to an equivalent receipt. Further details regarding the configuration can be found in the Supporting Information section S1.

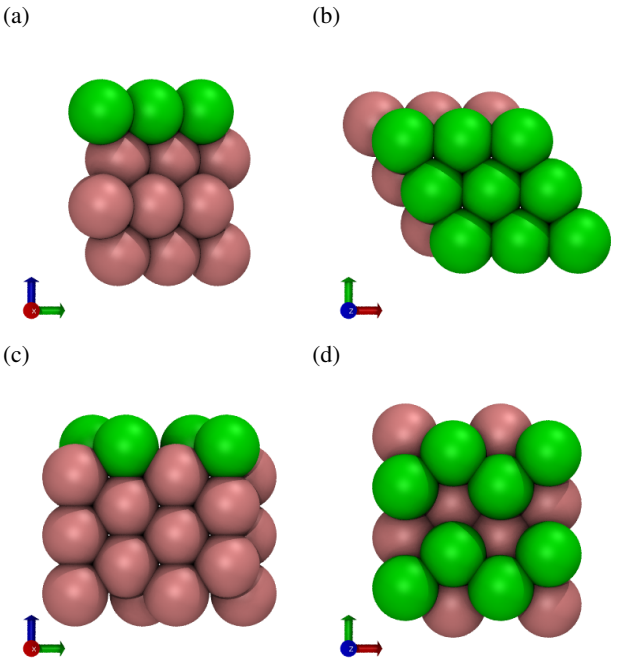

Figure 1. Structure of the cobalt slab, the first layer is in green while the others are in pink. (a) side view and (b) top view of surface Co(0001), (c) side view and (d) top view of surface Co(11$\bar{2}$0).

B. Molecular Mechanics

Molecular mechanics simulations were performed with a modified version of CP2K 9.1[60,61] using the smooth particle-mesh Ewald summation with the alpha parameter set to 0.36 Å^{-1}. A grid resolution of approximately 1 point per Å of the unit-cell length was employed. The standard scaling factors for 1-4 interaction were used: 0.5 for the van der Waals 1-4 interactions and 0.833 for the electrostatic 1-4 interactions.The GLJ cutoff was established at 4 Å for GLJ parameter fitting and set to 10 Å for ligand adsorption simulation. We have carefully tested whether the chosen system size is sufficient for fitting the parameters in Supporting Information section S3. The General AMBER Force Field (GAFF)[62] was employed for organic molecules, and RESP charges[63] were computed using the HF/6-31G* level of theory for the radical form (charge 0 with spin multiplicity 2). The Lennard–Jones parameters of cobalt were initially obtained from the Universal Force Field (UFF) force field[64] ($r = 1.436$ Å, $\varepsilon = 0.014$ kcal/mol). However, these parameters were subsequently modified during the fitting procedure explained in the next section. The charge of Co atoms is set to zero. To improve the description of the interaction of organic molecules with the cobalt surfaces, anisotropic attractive Gaussian potentials between surface Cobalt atoms (Co) and oxygen (O) of the organic molecules were added[40,41,65]. The general expression of the potential for a given Co-O interaction is as follows

$$V_{\mathrm{LJ}} + V_{\mathrm{Gauss}} = \sum_{i\in[O]} \sum_{j\in[Co]} \varepsilon_{\min} \left(\left(\frac{r_{\min}}{r_{ij}} \right)^{12} - 2 \left(\frac{r_{\min}}{r_{ij}} \right)^{6} \right) - \sum_{i\in[O]} \sum_{j\in[Co]} \varepsilon_{\mathrm{att}}\, e^{-b_{xy} r_{xy}^2}\, e^{-b_z r_z^2} \quad (1)$$

where r_{ij} is the distance between atoms i and j and $\varepsilon_{\min}$ is the minimum of the Lennard–Jones (LJ) energy well which is located at $r_{\min}$ and $\varepsilon_{\mathrm{att}}$ is the magnitude of the Gaussian attraction. r_{xy} and r_z are the Co-O distances in the (x,y) plane and the out-of-plane z direction, respectively. b_{xy} and b_z are the corresponding inverse width parameters of the Gaussian. This combination (Eq. 1) will be referred to as GLJ in this article.

For the MD simulations, a time step of 0.5 fs was used. These simulations were conducted in the NVT ensemble employing a Nose-Hoover thermostat with a time constant of the thermostat chain of 200 fs. An equilibration period of 100 ps was performed before the production run, which spanned 900 ps. Thus, the total simulation duration was 1 ns. Various temperatures were utilized, as outlined in Section D.

C. Fitting Procedure

Only the Co atoms of the first layer are involved in the GLJ potential while the atoms of the other layers are only described by the LJ potential. We initially calibrated the LJ parameters ($r_{\min}$, $\varepsilon_{\min}$) for the Co atom using the z-scan training set of the Co(0001) surface (see section S1.1). Subsequently, we applied the same LJ parameters for all Co atoms of both surfaces. Finally, we determined the Gaussian parameters for the attractive Co-O interaction ($\varepsilon_{\mathrm{att}}$, b_{xy}, b_z) separately for each surface. As a result, we derived the GLJ with five parameters for each surface. The optimization process employed an automatic fitting procedure with the simplex algorithm, implemented within the SIESTA package[66]. We have performed several hundreds of simplex optimizations with varying initial conditions in order to increase the likelihood of identifying the global minimum. The objective function of this fitting procedure was to minimize the root-mean-square deviation (RMSD) of adsorption energies across the training set. The DFT results are used as reference. To calculate the adsorption energy (E_{ads}), we determined the difference between the total energy of the complete system (E_{sys}) and the combined energies of the metal slab (E_{slab}) and the small molecule radical (E_{mol}) in the gas phase:

$$E_{ads} = E_{sys} - E_{mol} - E_{slab} \quad (2)$$

D. Application to Ligand Decorated Cobalt Surfaces

Once parametrized, Gaussian potentials are utilized to simulate two different cobalt facets decorated with laurate ligands ($C_{11}H_{23}COO\cdot$). The simulation model for the Co(0001) surface contained 576 cobalt atoms ($p(12\times12)$, 4 layers) with a simulation box measuring $29.64 \times 29.64 \times 80$ Å^3 (with angles α, β, γ = 90°, 90°, 120°). The Co(11$\bar{2}$0) surface was represented with 588 cobalt atoms ($p(14 \times 7)$, 6 layers) with a cuboid simulation box measuring $28.23 \times 29.94 \times 80$ Å^3.

Periodic boundary conditions were applied in all three directions. Laurate ligands were added in the simulation box using the Packmol software[67], maintaining a perpendicular distance of 2.5 Å from the cobalt surface. During this process, two oxygen atoms of each ligand were intentionally oriented towards the surface. The initial adsorbed structure was then subjected to a geometry optimization. Throughout the simulations, all cobalt atoms remained fixed. The optimized structure was utilized as the starting configuration for molecular dynamics simulations. We utilized a range of temperatures (301 K, 327 K, 353 K, 418 K, 448 K, and 573 K). Starting from room temperature at 301 K, we increased the temperature up to 448 K, which is the temperature employed by the experimental group for synthesizing these ligand-decorated Co nanoparticles. Additionally, we tested a higher temperature of 573 K, a temperature employed in experimental procedures to decompose the excess ligands.

To assess the influence of laurate ligand concentration on the two surfaces, we introduced various numbers of ligand (nb-L), see Table I. Based on our assumption that each ligand will bind to two surface cobalt atoms, a complete monolayer coverage (100 ML%) on our Co(0001) surface would require 72 ligands, while the Co(11$\bar{2}$0) surface would require 49 ligands. This corresponds to ligand concentrations of 9.46 nb-L/nm^2 and 5.8 nb-L/nm^2, respectively.

Table I. Investigated concentrations of ligands on Co(0001) and Co(11$\bar{2}$0) surfaces in terms of monolayers (ML) and numbers of ligands (L) per unit area.

Co(0001)			Co(11$\bar{2}$0)		
nb-L	ML%	nb-L/nm^2	nb-L	ML%	nb-L/nm^2
15	20	1.97	10	20	1.15
29	40	3.81	20	40	2.31
43	60	5.65	29	60	3.48
58	70	6.57	39	80	4.64
72	100	9.46	49	100	5.8

III. RESULTS AND DISCUSSION

A. Combination of Lennard–Jones and Gaussian Potentials

To create force field parameters between organic molecules and metal surfaces, the most common method is to employ Lennard–Jones (LJ) parameters and to apply combination rules between atoms to construct a LJ potential. This is typically the approach we employed for the Co-C and Co-H potentials combining the Universal Force Field (UFF) parameters for cobalt with the General Amber Force Field (GAFF) parameters for carbon and hydrogen.

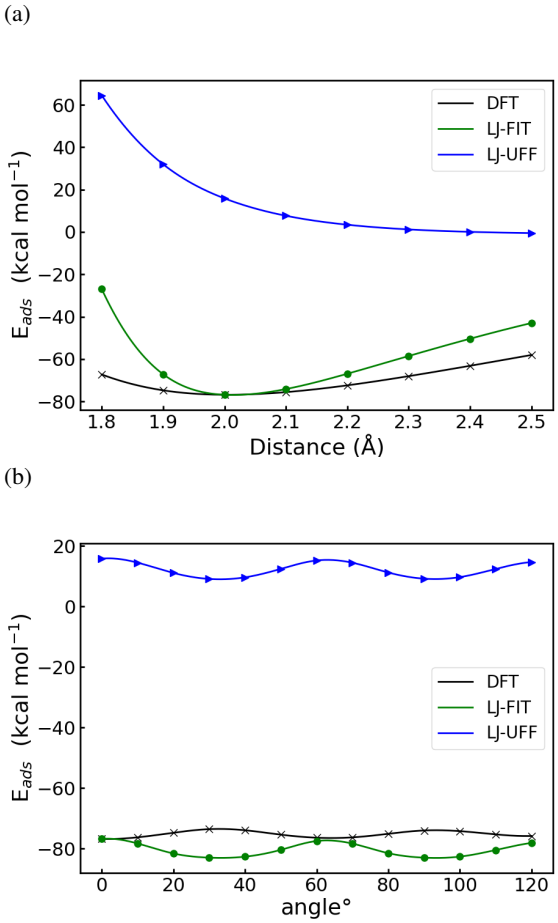

Figure 2. The adsorption energy of the acetyloxyl adsorbate on the Co(0001) surface was calculated using DFT (black curve), original LJ-UFF parameters (blue curve) and fitted LJ paramters LJ-FIT (green curve), while translating the adsorbed molecule along z-axis (a) and exploring the variation in the angle (ω) (b)

For the Co-O potential, the use of combination rule to build the LJ potential using LJ-UFF for Co (r = 1.436 Å and ε = 0.014 kcal/mol) results is a weakly binding potential. To assess the quality of this potential, we plotted the adsorption energy of the acetyloxyl adsorbated on the Co(0001) surface calculated with LJ-UFF and with DFT. Figure 2.a is the z-scan training set and Figure 2.b is the angle (ω) rotation set (see Figure S1 for structures). A notable difference between the DFT result (black curve) and the LJ-UFF result (blue curve) is observed. This is due to the considerable strength of the interaction between the ligand and the cobalt surface. Then, we attempted to match the DFT potential by exclusively tuning the LJ-UFF parameters. This resulted in the LJ-FIT parameters of r = 0.452 Å and ε = 903 kcal/mol. Owing to the intrinsic limitations of the LJ functional form, the curvature

of the z-scan is not reproduced accurately as depicted by the gree curve in Figure 2.a. Furthermore, the rotational profile of LJ force fields produced qualitatively incorrect minima (Figure 2.b). None of these LJ potentials (LJ-UFF and LJ-FIT) can correctly describe the site preference of the strong Co-carboxylate chemisorption and the diffusion parallel to the Co surface.

It becomes evident that relying solely on a LJ potential, which normally accounts for a few kcal/mol, is inadequate to describe such a strong interaction. The interaction occurring between the oxygen and cobalt atoms nearly reaches the threshold of forming a chemical bond. Despite this, we have chosen not to restrict the ligand with a harmonic bond since it would prevent diffusion. By adopting the GLJ approach, we allow the ligand to diffuse along the x, y and possibly z axes.

B. Quality of the Parametrization

The GLJ force field for Co-O is fitted using $C_2H_3COO\cdot$ on two different surfaces of Co: (i) the compact planar surface Co(0001) and (ii) the Co(11$\bar{2}$0) which is more corrugated and exhibits zig-zag rows of Co (Figure 1). In both cases, all surface Co atoms are equivalent. According to DFT geometry optimization, the carboxyl radical stands perpendicular to the surface plane, each oxygen being bonded to one surface Co at the ontop site. This agrees well with the result obtained by Farkaš et al. who have identified the bidentate mode as the most stable adsorption mode[68]. The adsorption is stronger on the corrugated surface compared to Co(0001) (-94.4 kcal/mol vs -76.8 kcal/mol), which is also accompanied by a shorter Co-O distance (1.94 Å vs. 2.00 Å). This equilibrium distance agrees well with previous DFT calculations[68].

When we began the fitting process using the GLJ model with the z-scan training set on surface Co(0001) and the default UFF LJ parameters (r = 1.436 Å and ε = 0.014 kcal/mol), accurately representing the short-distance behaviors was a challenge. To address this, we initially modified the LJ parameters of Co to r = 1.2 Å and ε = 0.014 kcal/mol. This modification enhanced our ability to represent the short-distance potential more accurately and to exert a gentler effect on the xy plane (see Figure S3). We employed the same LJ parameters for the Co(11$\bar{2}$0) surface, whereas we have chosen to fit specific parameters for attractive Gaussian for the two surfaces. The fitted parameters of the attractive Gaussian are given in Table II. The other ligand force-field parameters are given in SI Section S2.

Table II. Fitted Parameters for the Attractive Gaussian Potential for Co and O of COO.

System	ε_{att} (kcal/mol)	b_{xy} (Å^{-2})	b_z (Å^{-2})
Co(0001)-O	55.26	0.62	0.11
Co(11$\bar{2}$0)-O	73.66	0.42	0.14

The adsorption energies of all 198 structures of acetyloxyl radical molecule on Co(0001) surfaces calculated with DFT and MM are shown in Figure 3. The interaction energy is systematically too weak for the original LJ-UFF parameters with a RMSD over the entire set of 75.9 kcal/mol. The result with only tuned LJ parameters (LJ-FIT) also has a better performance with a RMSD of 19.3 kcal/mol, but shows qualitative errors considering the lack of correlation between DFT and LJ-FIT in Figure 3a. Once supplemented by an attractive Gaussian, GLJ results are much closer to DFT with a RMSD 2.6 kcal/mol, which corresponding to a root mean square percentage deviation (RMPD) of 4.0%. We observed that structures that are very close to metal surface with z(Co-O) = 1.8 Å (blue points) do not correlate well with the DFT reference values. We have identified this regime as problematic in our previous work on GLJ for oxide surfaces:[43] at short distances, the repulsive wall of the Lennard–Jones potential does not allow for a faithful description of the energy landscape. More surprisingly, structures that are far from surface (z(Co-O) = 2.5 Å) (green points) have, sometimes, also larger errors than

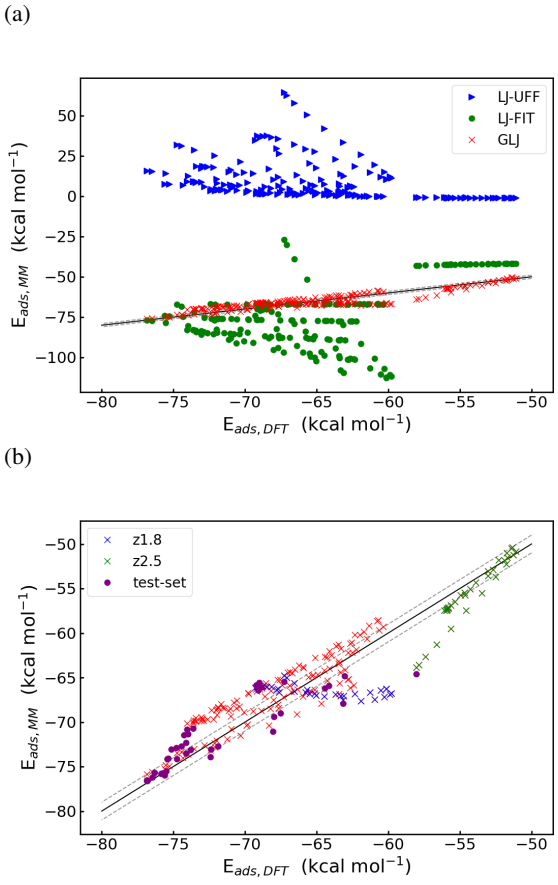

Figure 3. Correlation of adsorption energies between DFT reference data (black curve) and MM level methods for the adsorption of a single acetyloxyl radical molecule on Co(0001) surface for various adsorption conformations. (a) Comparison of the LJ (blue stars) and GLJ (red crosses) for the training set. (b) The GLJ results for the training set (crosses) and the test set (purple circles). The training set conformations at an O-Co distance (z) of 1.8 Å, and 2.5 Å are highlighted in blue and green, respectively.

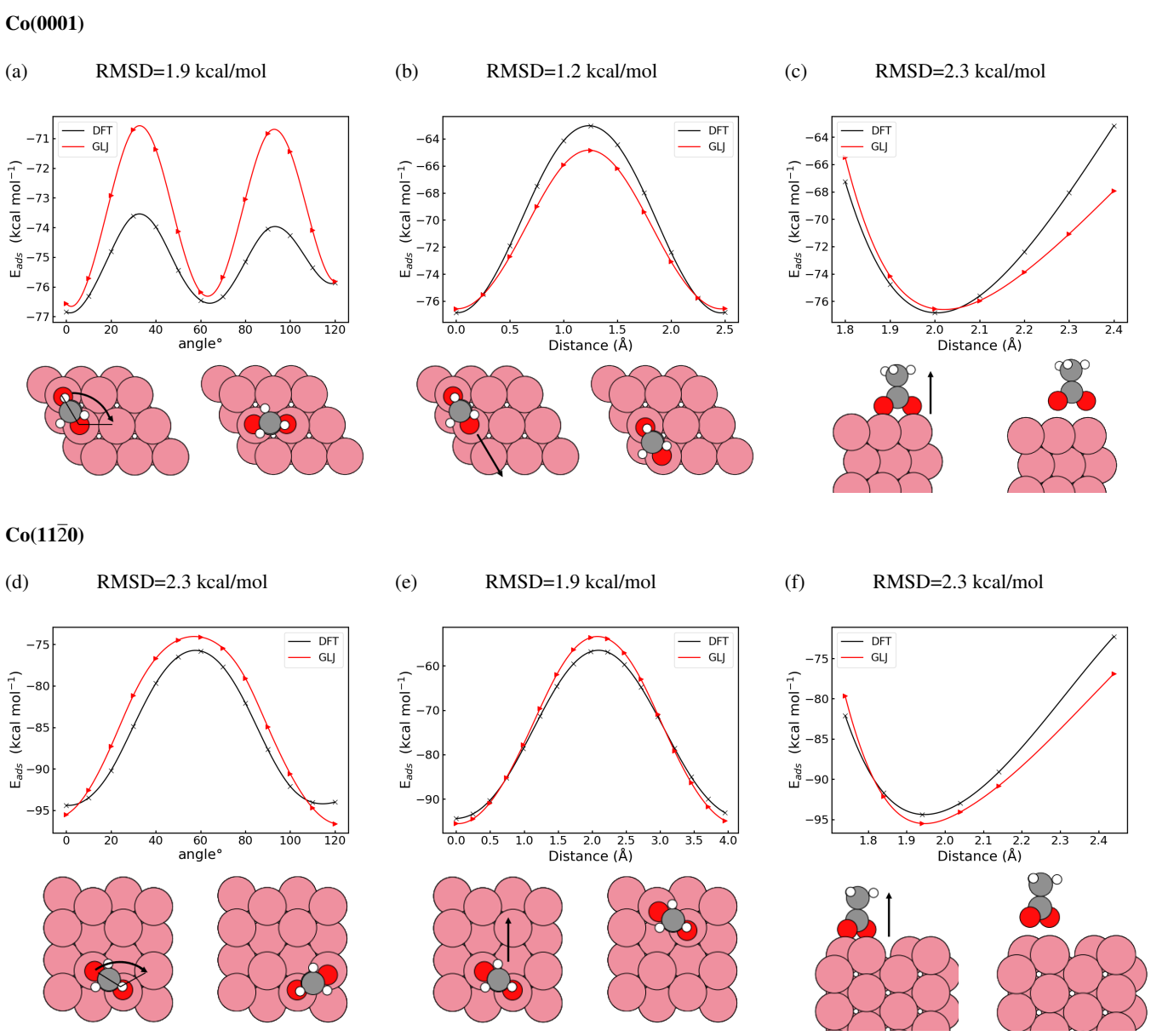

Figure 4. The adsorption energy of the acetyloxyl adsorbate on the Co(0001) (top row) and Co(11$\bar{2}$0) surface (bottom row) was calculated using DFT (black curve) and GLJ (red curve), while exploring the variation in the angle (a,d) and the translation of the adsorbed molecule along the *y*-axis (b,e) and *z*-axis (c,e). The profiles found along the *x*-axis are shown in Figure S4.

other structures (Figure 3.b). This is probably related to the near-covalent nature of the interaction between R-COO and the metal surface. The results of the test set (20 structures) are plotted in (Figure 3.b) as purple circles. Here again, we found a RMSD 2.0 kcal/mol with RMPD 3.1 %, which further validated our parameters. Similar fitting results were obtained for Co(11$\bar{2}$0) surface with RMSD around 3.6 kcal/mol and RMPD of 4.9%. The details are described in the supporting information section S4.1, see also Figure S7.

To perform a more detailed analysis of the performance of GLJ, we plotted the results from the test set in Figure 4 for the two surfaces. The test set involved scanning the angle (ω), two translations parallel to the surface plane (x, y) and one perpendicular to the surface (along the z axe of the cell). The specific values are provided in the SI section S1. Besides, to better understand the impact of combining LJ and Gaussian potentials, the respective components are plotted for both the z-distance scan and the angle scan potential energy in Figure S3.

On both surfaces, the GLJ results (red curve) agree well with the DFT results (black curve). Both curves displayed similar maxima and minima. The root mean square devia-

tion (RMSD) for the structures in Figure 4 were determined to be about 2.3 kcal/mol, excepted the diffusion profile along the Co zig-zag rows of the Co(11$\bar{2}$0) (shown in Figure S4), where GLJ underestimates the diffusion barrier. This underestimation is important to keep in mind for the discussion of the mobility of the ligands on the surfaces: The GLJ barriers are still high enough to feature very low diffusion coefficients (see Figure S13 through S20). These results ensure that we can accurately simulate the structure and dynamics of a carboxylate layer not only in the z direction but also considering the translation barrier in the x, y direction, and that we should be able to accurately differentiate the behavior on the two surfaces.

C. Investigation of the Ligand Dynamics

We now consider laurate films of various concentrations on the two surfaces to determine if corrugation of the surface plays an important role on the structure and dynamics of the film.

Thanks to the GLJ force field, the laurate ligands are stably adsorbed on the cobalt surface during the dynamics. Nevertheless, the GLJ energy expression allows the ligands to move parallel to the surface and also adapt their out-of-plane distance to the corrugation of the potential energy surface. After geometry optimization, the oxygen atoms were found to be adsorbed at approximately 2 Å from the Co surface, which is in good agreement with the DFT result. Structures with different ligand coverages on Co(0001) after 1 ns molecular dynamics simulations at 449 K are shown in Figure 5. The equivalent structures for the Co(11$\bar{2}$0) surface are shown in Figure S8.

To characterize the order of the ligands, we calculated the angle between the surface's normal vector and the vector connecting the first and last carbon atom of the aliphatic chain. We averaged the angle of each ligand throughout the simulation time and subsequently computed the average angle across all ligands. If the average value of this angle is close to 0, it indicates that the ligands are parallel to the surface normal and well-organized. As depicted in the Figure 6, an increase in ligand concentration leads to a decrease in the average angle on both surfaces. This indicates that the ligands exhibit a more organized structure, adopting a standing-up orientation at higher concentrations, as illustrated in Figure 5. Additionally, we observed a decrease in the angle as the temperature increased (as illustrated on Co(0001) in Figure 6.a). This phenomenon can be attributed to the increased thermal motion of the aliphatic chain, which leads to a more "cone-shaped" space requirement as temperature increases, effectively increasing the steric repulsion among the different ligands. To assess the influence of the metallic surface structure on the organic film structuring, we plotted the data at 449 K for both surfaces in Figure 6.b. There is no significant difference in the average angle between these two surfaces. This suggests that the arrangement of the aliphatic chains is not influenced by the surface structure but more by the concentration of laurate ligands.

We assessed the mobility of the ligands by calculating the root mean square fluctuation (RMSF) of the oxygen pairs of each ligand and averaging these values across all ligands: the higher the RMSF, the higher the mobility of ligands is. As shown in Figure 7.a, as the concentration increases, the RMSF decreases due to limited space for movement on both surfaces. Conversely, at lower concentrations, there is still room for mobility, leading to an increase in RMSF as the temperature rises (see Figure S10). This behaviour may be analysed as a shift towards a subdiffusive regime at high concentration. However, a careful analysis of the time evolution of the average Mean Square Displacement (MSD) of the ligands clearly shows a behaviour that is not compatible with a random subdiffusive regime (see Figure S12). Besides, the time evolution of the MSD of each ligand exhibits jumps that are characteristic of an activated diffusion (see Figure S13 through S20 in the SI). This can be put in regards with the corrugated Co-O potentials with in-plane barriers of 10 to 20 kcal/mol (see Figure 4). In addition, we observed a difference in mobility between the Co(11$\bar{2}$0) and Co(0001) surfaces (Figure 7a). At lower concentrations, the RMSF on the Co(11$\bar{2}$0) surface was approximately 1 Å lower compared to the Co(0001) surface. To gain a deeper understanding of the difference in RMSF between the two surfaces, we plotted the mobility along the x, y, and z directions in Figure 7b, c, and Figure S10b, respectively. The mobility in z direction is small (~ 0.1 Å) and identical for both surfaces. This can be understood when considering the strong adsorption of the molecule seen in Figure 4. While on Co(0001) the x and y directions are equivalent (with Co-Co distances of 2.47 Å), this is not the case for Co(11$\bar{2}$0), where the zig-zag rows along x-direction feature small Co-Co distance, but those rows are spaced by about 4.28 Å in the y-direction. This difference can be related to the ~ 10 kcal/mol higher energy barriers for in-plane diffusion when comparing Co(11$\bar{2}$0) and Co(0001) (Figure 4 and Figure S4), a barrier which makes also the minimum less broad. In line with those observations, the mobility in x-direction is very similar for both surfaces, while the mobility in y-direction is almost zero for Co(11$\bar{2}$0). We observed a similar trend for other temperatures as well (Figure S11). In a nutshell, the surface-ligand interaction modulates the in-plane diffusion yielding to an activated diffusion rather than a subdiffusive random diffusion, even at high concentration.

IV. CONCLUSIONS

We have parametrized a simple force field to investigate ligand-decorated cobalt surfaces. The model was designed to accurately capture the essential features of nanorods which mostly expose the Co(0001) and Co(11$\bar{2}$0) surfaces. To achieve an accurate description of ligand adsorption and dynamics on the surface, an attractive Gaussian potential is added to supplement a Lennard–Jones potential, leading to the GLJ functional form that was previously used for oxide surfaces. The inclusion of the attractive Gaussian between the oxygen and Co atoms achieves a quantitative and qualitative improvement in terms of adsorption energies and preferred ad-

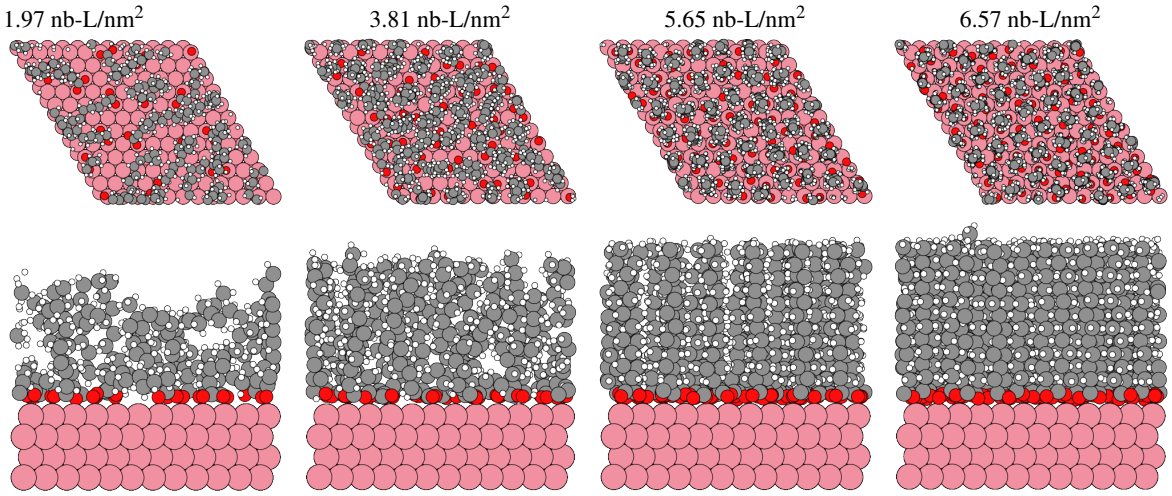

Figure 5. Top and side views of different number of ligands on Co(0001) surface at 449 K after an MD simulation of 1 ns.

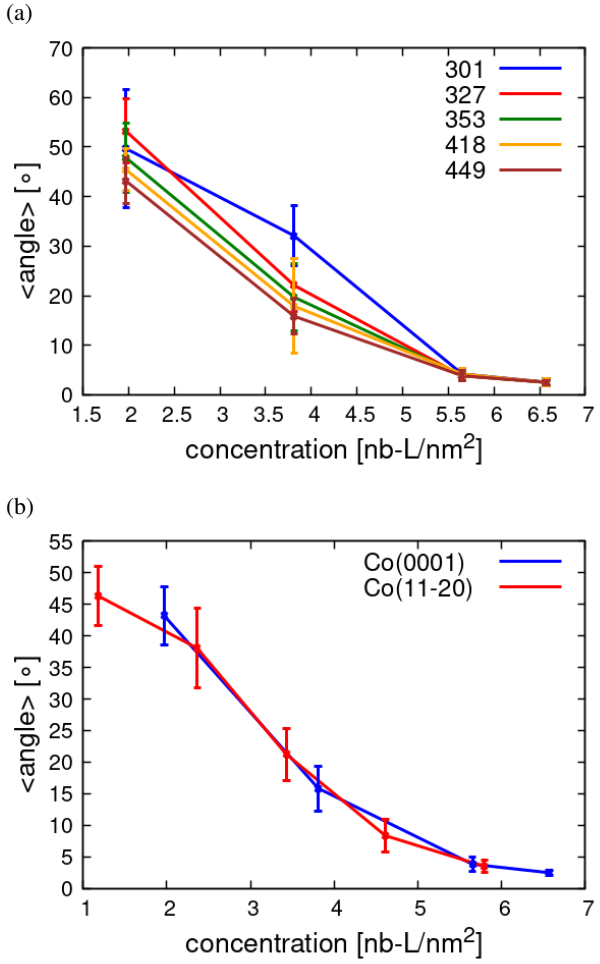

Figure 6. Analysis of the alkyl-chain order (a) on Co(0001) surface at different temperatures (labels, in Kelvin) and (b) on Co(0001) and Co(11$\bar{2}$0) surface at 449 K. Error bars represent the standard deviation, which indicates the fluctuation of the average angle over time.

sorption configurations compared to use of only an LJ potential. The root mean square deviation (RMSD) values for GLJ are 2 to 4 kcal/mol and the root mean square percentage deviation is in the range of 3 to 5 % depending on the surface. Moreover, GLJ reproduces diffusion barriers faithfully compared to DFT data.

The application of GLJ to simulate ligand-decorated cobalt surfaces at various temperatures allows for an analysis of the impact of ligand concentration on the film's order. Distinct mobility in the x and y directions is observed for Co(11$\bar{2}$0), attributed to the varying corrugation "along" the zig-zag lines compared to perpendicular to them. However, at the relevant temperatures, diffusion seems to be an activated process, i.e., a rare event in the absence of an external stimulus. Our parametrization paves the way for future studies of the diffusion of target molecules through the ligand-decorated surface and determining which surface is most accessible to target molecules.

ACKNOWLEDGMENTS

This work is part of the projcet GLYNANO funded by the French National Reserach Agency(ANR-21-CE43-0016). The authors thank the SYSPROD project and AXELERA Pôle de Compétitivité for financial support (PSMN Data Center).

DATA AVAILABILITY STATEMENT

The data that support the findings of this study are available within the article, its supplementary material and on `nomad-lab.eu`: The DFT computations are available under `10.17172/NOMAD/2023.08.08-1`, while xyz structures of the training set and test set are also provided as (structures.zip) attached to this article. Details of construction of training set and test set, force field parameters of the system, results on Co(11$\bar{2}$0) and the root mean square fluctuations and diffusion

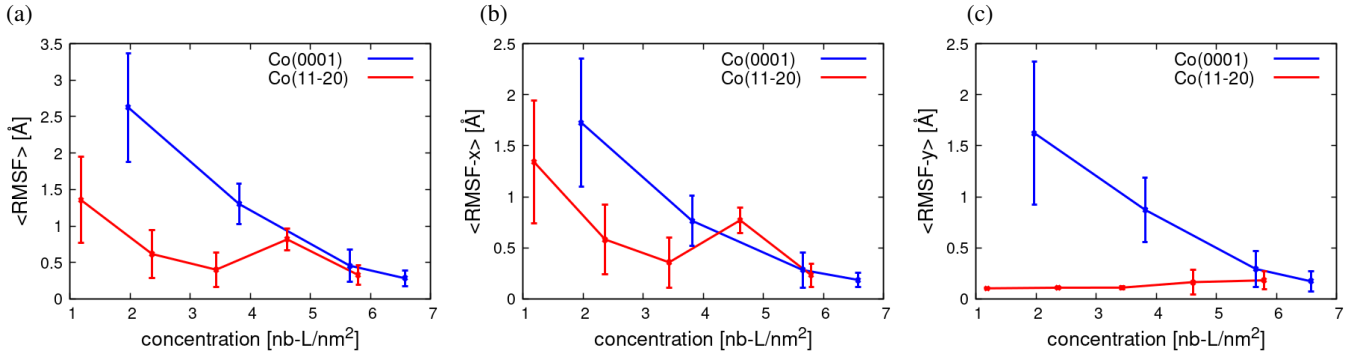

Figure 7. Root mean square fluctuations (RMSF) of ligands (a) all, (b) x and (c) y directions on Co(0001) (blue) and Co(11$\bar{2}$0) (red) surface at 449 K.

constants of ligands in x, y and z direction for both surface are found in the supplementary material (PDF). Parameters files are provided together with the xyz structures.

V. AUTHOR DECLARATION

The authors have no conflicts to disclose.

REFERENCES

[1] Z. Tang and S. Li, "A review of recent developments of friction modifiers for liquid lubricants (2007-present)," CURRENT OPINION IN SOLID STATE & MATERIALS SCIENCE **18**, 119–139 (2014).

[2] R. Shi, Z. Shen, Q. Yue, and Y. Zhao, "Advances in functional organic material-based interfacial engineering on metal anodes for rechargeable secondary batteries," Nanoscale **15**, 9256–9289 (2023).

[3] M. Krasowska, J. Zawala, B. H. Bradshaw-Hajek, J. K. Ferri, and D. A. Beattie, "Interfacial characterisation for flotation: 1. solid-liquid interface," Current Opinion in Colloid & Interface Science **37**, 61–73 (2018).

[4] M. Cusack and A. Freer, "Biomineralization: Elemental and Organic Influence in Carbonate Systems," Chemical Reviews **108**, 4433–4454 (2008).

[5] J. M. Tour, "Molecular electronics. synthesis and testing of components," Accounts of Chemical Research **33**, 791–804 (2000).

[6] Q. Yun, Y. Ge, B. Huang, Q. Wa, and H. Zhang, "Ligand-Assisted Phase Engineering of Nanomaterials," Accounts of Chemical Research **56**, 1780–1790 (2023).

[7] Y. Xia, Y. Xiong, B. Lim, and S. E. Skrabalak, "Shape-Controlled Synthesis of Metal Nanocrystals: Simple Chemistry Meets Complex Physics?" Angewandte Chemie International Edition **48**, 60–103 (2009).

[8] S. T. Marshall and J. W. Medlin, "Surface-level mechanistic studies of adsorbate–adsorbate interactions in heterogeneous catalysis by metals," Surface Science Reports **66**, 173–184 (2011).

[9] L. O. Mark, C. Zhu, J. W. Medlin, and H. Heinz, "Understanding the Surface Reactivity of Ligand-Protected Metal Nanoparticles for Biomass Upgrading," ACS Catalysis **10**, 5462–5474 (2020).

[10] J. Yan, B. K. Teo, and N. Zheng, "Surface Chemistry of Atomically Precise Coinage–Metal Nanoclusters: From Structural Control to Surface Reactivity and Catalysis," Accounts of Chemical Research **51**, 3084–3093 (2018).

[11] S. Kango, S. Kalia, A. Celli, J. Njuguna, Y. Habibi, and R. Kumar, "Surface modification of inorganic nanoparticles for development of organic–inorganic nanocomposites—A review," Progress in Polymer Science Topical Issue on Polymer Hybrids, **38**, 1232–1261 (2013).

[12] H. Heinz, C. Pramanik, O. Heinz, Y. Ding, R. K. Mishra, D. Marchon, R. J. Flatt, I. Estrela-Lopis, J. Llop, S. Moya, and R. F. Ziolo, "Nanoparticle decoration with surfactants: Molecular interactions, assembly, and applications," Surface Science Reports **72**, 1–58 (2017).

[13] S. H. Deshmukh, S. Chatterjee, D. Ghosh, and S. Bagchi, "Ligand Dynamics Time Scales Identify the Surface–Ligand Interactions in Thiocyanate-Capped Cadmium Sulfide Nanocrystals," The Journal of Physical Chemistry Letters **13**, 3059–3065 (2022).

[14] R. V. Mom, S. T. A. G. Melissen, P. Sautet, J. W. M. Frenken, S. N. Steinmann, and I. M. N. Groot, "The Pressure Gap for Thiols: Methanethiol Self-Assembly on Au(111) from Vacuum to 1 bar," J. Phys. Chem. C **123**, 12382–12389 (2019).

[15] W. Chen, S. Hong, H. B. Li, H. Q. Luo, M. Li, and N. B. Li, "Protection of copper corrosion in 0.5M NaCl solution by modification of 5-mercapto-3-phenyl-1,3,4-thiadiazole-2-thione potassium self-assembled monolayer," Corrosion Science **61**, 53–62 (2012).

[16] K. Kaźmierczak, D. Yi, A. Jaud, P.-F. Fazzini, M. Estrader, G. Viau, P. Decorse, J.-Y. Piquemal, C. Michel, M. Besson, K. Soulantica, and N. Perret, "Influence of Capping Ligands on the Catalytic Performances of Cobalt Nanoparticles Prepared with the Organometallic Route," The Journal of Physical Chemistry C **125**, 7711–7720 (2021).

[17] G. Martí, L. Mallón, N. Romero, L. Francàs, R. Bofill, K. Philippot, J. García-Antón, and X. Sala, "Surface-functionalized nanoparticles as catalysts for artificial photosynthesis," Advanced Energy Materials **13**, 2300282 (2023), https://onlinelibrary-wiley-com.inc.bib.cnrs.fr/doi/pdf/10.1002/aenm.202300282.

[18] M. A. Ortuño and N. López, "Reaction mechanisms at the homogeneous–heterogeneous frontier: insights from first-principles studies on ligand-decorated metal nanoparticles," Catalysis Science & Technology **9**, 5173–5185 (2019).

[19] Z. Hens and J. C. Martins, "A Solution NMR Toolbox for Characterizing the Surface Chemistry of Colloidal Nanocrystals," Chemistry of Materials **25**, 1211–1221 (2013).

[20] M. Xue, J. Sampath, R. N. Gebhart, H. J. Haugen, S. P. Lyngstadaas, J. Pfaendtner, and G. Drobny, "Studies of Dynamic Binding of Amino Acids to TiO2 Nanoparticle Surfaces by Solution NMR and Molecular Dynamics Simulations," Langmuir **36**, 10341–10350 (2020).

[21] S. Cosseddu, R. Pascazio, C. Giansante, L. Manna, and I. Infante, "Ligand dynamics on the surface of CdSe nanocrystals," Nanoscale **15**, 7410–7419 (2023).

[22] A. S. Pensado and A. A. H. Pádua, "Solvation and Stabilization of Metallic Nanoparticles in Ionic Liquids," Angewandte Chemie International Edition **50**, 8683–8687 (2011).

[23] R. Réocreux, T. Jiang, M. Iannuzzi, C. Michel, and P. Sautet, "Structuration and dynamics of interfacial liquid water at hydrated γ-alumina determined by ab initio molecular simulations: Implications for nanoparticle stability," ACS Applied Nano Materials **1**, 191–199 (2018).

[24] O. Drecun, A. Striolo, C. Bernardini, and M. Sarwar, "Hydration Structures on γ-Alumina Surfaces With and Without Electrolytes Probed by Atomistic Molecular Dynamics Simulations," The Journal of Physical Chemistry B **126**, 9105–9122 (2022).

[25] W. Kaiser, D. Ricciarelli, E. Mosconi, A. A. Alothman, F. Ambrosio, and F. De Angelis, "Stability of Tin- versus Lead-Halide Perovskites: Ab Initio Molecular Dynamics Simulations of Perovskite/Water Interfaces," The

Journal of Physical Chemistry Letters , 2321–2329 (2022).
[26]M. Y. Sengul, C. A. Randall, and A. C. T. van Duin, "ReaxFF Molecular Dynamics Study on the Influence of Temperature on Adsorption, Desorption, and Decomposition at the Acetic Acid/Water/ZnO(10-10) Interface Enabling Cold Sintering," ACS Applied Materials & Interfaces **10**, 37717–37724 (2018).
[27]J. Rey, P. Clabaut, R. Réocreux, S. N. Steinmann, and C. Michel, "Mechanistic investigation and free energies of the reactive adsorption of ethanol at the alumina/water interface," The Journal of Physical Chemistry C **126**, 7446–7455 (2022).
[28]J. Aufort, A. Schuitemaker, R. Green, R. Demichelis, P. Raiteri, and J. D. Gale, "Determining the Adsorption Free Energies of Small Organic Molecules and Intrinsic Ions at the Terrace and Steps of Calcite," Crystal Growth & Design **22**, 1445–1458 (2022).
[29]R. Réocreux, E. Girel, P. Clabaut, A. Tuel, M. Besson, A. Chaumonnot, A. Cabiac, P. Sautet, and C. Michel, "Reactivity of shape-controlled crystals and metadynamics simulations locate the weak spots of alumina in water," Nature Communications **10**, 3139 (2019).
[30]N. Siemer, D. Munoz-Santiburcio, and D. Marx, "Solvation-Enhanced Oxygen Activation at Gold/Titania Nanocatalysts," Acs Catalysis **10**, 8530–8534 (2020).
[31]M. Karplus and J. A. McCammon, "Molecular dynamics simulations of biomolecules," Nature Structural Biology **9**, 646–652 (2002).
[32]H. Heinz, T.-J. Lin, R. Kishore Mishra, and F. S. Emami, "Thermodynamically Consistent Force Fields for the Assembly of Inorganic, Organic, and Biological Nanostructures: The INTERFACE Force Field," Langmuir **29**, 1754–1765 (2013).
[33]O. T. Unke, S. Chmiela, H. E. Sauceda, M. Gastegger, I. Poltavsky, K. T. Schütt, A. Tkatchenko, and K.-R. Müller, "Machine Learning Force Fields," Chemical Reviews **121**, 10142–10186 (2021).
[34]M. F. C. Andrade, H.-Y. Ko, L. Zhang, R. Car, and A. Selloni, "Free energy of proton transfer at the water–TiO2 interface from ab initio deep potential molecular dynamics," Chemical Science **11**, 2335–2341 (2020).
[35]F. Noé, A. Tkatchenko, K.-R. Müller, and C. Clementi, "Machine Learning for Molecular Simulation," Annual Review of Physical Chemistry **71**, 361–390 (2020).
[36]V. Quaranta, J. Behler, and M. Hellström, "Structure and Dynamics of the Liquid–Water/Zinc-Oxide Interface from Machine Learning Potential Simulations," The Journal of Physical Chemistry C **123**, 1293–1304 (2019).
[37]M. Eckhoff and J. Behler, "Insights into lithium manganese oxide–water interfaces using machine learning potentials," The Journal of Chemical Physics **155**, 244703 (2021).
[38]F. Iori, R. Di Felice, E. Molinari, and S. Corni, "GolP: An atomistic force-field to describe the interaction of proteins with Au(111) surfaces in water," Journal of Computational Chemistry **30**, 1465–1476 (2009).
[39]L. B. Wright, P. M. Rodger, S. Corni, and T. R. Walsh, "GolP-CHARMM: First-Principles Based Force Fields for the Interaction of Proteins with Au(111) and Au(100)," Journal of Chemical Theory and Computation **9**, 1616–1630 (2013).
[40]S. N. Steinmann, R. Ferreira De Morais, A. W. Götz, P. Fleurat-Lessard, M. Iannuzzi, P. Sautet, and C. Michel, "Force Field for Water over Pt(111): Development, Assessment, and Comparison," Journal of Chemical Theory and Computation **14**, 3238–3251 (2018).
[41]P. Clabaut, P. Fleurat-Lessard, C. Michel, and S. N. Steinmann, "Ten Facets, One Force Field: The GAL19 Force Field for Water–Noble Metal Interfaces," Journal of Chemical Theory and Computation **16**, 4565–4578 (2020).
[42]P. Clabaut, M. Beisert, C. Michel, and S. N. Steinmann, "Beyond single-crystal surfaces: The GAL21 water/metal force field," The Journal of Chemical Physics **157**, 194705 (2022).
[43]J. Rey, S. Blanck, P. Clabaut, S. Loehlé, S. N. Steinmann, and C. Michel, "Transferable gaussian attractive potentials for organic/oxide interfaces," The Journal of Physical Chemistry B **125**, 10843–10853 (2021), https://doi.org/10.1021/acs.jpcb.1c05156.
[44]K. Ait Atmane, C. Michel, J.-Y. Piquemal, P. Sautet, P. Beaunier, M. Giraud, M. Sicard, S. Nowak, R. Losno, and G. Viau, "Control of the anisotropic shape of cobalt nanorods in the liquid phase: from experiment to theory... and back," Nanoscale **6**, 2682–2692 (2014).
[45]K. De Nolf, S. M. Cosseddu, J. J. Jasieniak, E. Drijvers, J. C. Martins, I. Infante, and Z. Hens, "Binding and Packing in Two-Component Colloidal Quantum Dot Ligand Shells: Linear versus Branched Carboxylates," Journal of the American Chemical Society **139**, 3456–3464 (2017).
[46]K. Kaźmierczak, R. K. Ramamoorthy, A. Moisset, G. Viau, A. Viola, M. Giraud, J. Peron, L. Sicard, J.-Y. Piquemal, M. Besson, N. Perret, and C. Michel, "Importance of the decoration in shaped cobalt nanoparticles in the acceptor-less secondary alcohol dehydrogenation," Catalysis Science & Technology **10**, 4923–4937 (2020).
[47]K. Kaźmierczak, D. Yi, A. Jaud, P.-F. Fazzini, M. Estrader, G. Viau, P. Decorse, J.-Y. Piquemal, C. Michel, M. Besson, K. Soulantica, and N. Perret, "Influence of capping ligands on the catalytic performances of cobalt nanoparticles prepared with the organometallic route," The Journal of Physical Chemistry C **125**, 7711–7720 (2021).
[48]J. C. Love, L. A. Estroff, J. K. Kriebel, R. G. Nuzzo, and G. M. Whitesides, "Self-Assembled Monolayers of Thiolates on Metals as a Form of Nanotechnology," Chemical Reviews **105**, 1103–1170 (2005).
[49]M. Makosch, W.-I. Lin, V. Bumbálek, J. Sá, J. W. Medlin, K. Hungerbühler, and J. A. van Bokhoven, "Organic Thiol Modified Pt/TiO2 Catalysts to Control Chemoselective Hydrogenation of Substituted Nitroarenes," ACS Catalysis **2**, 2079–2081 (2012).
[50]S. Kunz, P. Schreiber, M. Ludwig, M. M. Maturi, O. Ackermann, M. Tschurl, and U. Heiz, "Rational design, characterization and catalytic application of metal clusters functionalized with hydrophilic, chiral ligands: a proof of principle study," Physical Chemistry Chemical Physics **15**, 19253–19261 (2013).
[51]L. Jin, B. Liu, S. S. Duay, and J. He, "Engineering Surface Ligands of Noble Metal Nanocatalysts in Tuning the Product Selectivity," Catalysts **7**, 44 (2017).
[52]J. J. Sims, C. A. Ould Hamou, R. Réocreux, C. Michel, and J. B. Giorgi, "Adsorption and decomposition of formic acid on cobalt (0001)," The Journal of Physical Chemistry C **122**, 20279–20288 (2018).
[53]G. Kresse and J. Furthmüller, "Efficient iterative schemes for *ab initio* total-energy calculations using a plane-wave basis set," Physical Review B **54**, 11169–11186 (1996).
[54]G. Kresse and J. Hafner, "*Ab initio* molecular dynamics for liquid metals," Physical Review B **47**, 558–561 (1993).
[55]J. P. Perdew, K. Burke, and M. Ernzerhof, "Generalized Gradient Approximation Made Simple," Physical Review Letters **77**, 3865–3868 (1996).
[56]S. N. Steinmann and C. Corminboeuf, "Comprehensive Benchmarking of a Density-Dependent Dispersion Correction," Journal of Chemical Theory and Computation **7**, 3567–3577 (2011).
[57]S. Gautier, S. N. Steinmann, C. Michel, P. Fleurat-Lessard, and P. Sautet, "Molecular adsorption at Pt(111). How accurate are DFT functionals?" Physical Chemistry Chemical Physics **17**, 28921–28930 (2015).
[58]P. E. Blöchl, "Projector augmented-wave method," Physical Review B **50**, 17953–17979 (1994).
[59]G. Kresse and D. Joubert, "From ultrasoft pseudopotentials to the projector augmented-wave method," Physical Review B **59**, 1758–1775 (1999).
[60]J. Hutter, M. Iannuzzi, F. Schiffmann, and J. VandeVondele, "cp2k: atomistic simulations of condensed matter systems," WIREs Computational Molecular Science **4**, 15–25 (2014).
[61]T. D. Kühne, M. Iannuzzi, M. Del Ben, V. V. Rybkin, P. Seewald, F. Stein, T. Laino, R. Z. Khaliullin, O. Schütt, F. Schiffmann, D. Golze, J. Wilhelm, S. Chulkov, M. H. Bani-Hashemian, V. Weber, U. Borštnik, M. Taillefumier, A. S. Jakobovits, A. Lazzaro, H. Pabst, T. Müller, R. Schade, M. Guidon, S. Andermatt, N. Holmberg, G. K. Schenter, A. Hehn, A. Bussy, F. Belleflamme, G. Tabacchi, A. Glöß, M. Lass, I. Bethune, C. J. Mundy, C. Plessl, M. Watkins, J. VandeVondele, M. Krack, and J. Hutter, "CP2K: An electronic structure and molecular dynamics software package - Quickstep: Efficient and accurate electronic structure calculations," The Journal of Chemical Physics **152**, 194103 (2020).
[62]J. Wang, R. M. Wolf, J. W. Caldwell, P. A. Kollman, and D. A. Case, "Development and testing of a general amber force field," Journal of Computational Chemistry **25**, 1157–1174 (2004).
[63]P. Cieplak, W. D. Cornell, C. Bayly, and P. A. Kollman, "Application of the multimolecule and multiconformational RESP methodology to biopolymers: Charge derivation for DNA, RNA, and proteins," Journal of Computational Chemistry **16**, 1357–1377 (1995).
[64]A. K. Rappe, C. J. Casewit, K. S. Colwell, W. A. Goddard, and W. M. Skiff, "UFF, a full periodic table force field for molecular mechanics and molecular dynamics simulations," Journal of the American Chemical Society **114**,

10024–10035 (1992).
[65] J. Rey, S. Blanck, P. Clabaut, S. Loehlé, S. N. Steinmann, and C. Michel, "Transferable Gaussian Attractive Potentials for Organic/Oxide Interfaces," The Journal of Physical Chemistry B **125**, 10843–10853 (2021).
[66] J. M. Soler, E. Artacho, J. D. Gale, A. García, J. Junquera, P. Ordejón, and D. Sánchez-Portal, "The SIESTA method for ab initio order-N materials simulation," Journal of Physics: Condensed Matter **14**, 2745 (2002).
[67] L. Martínez, R. Andrade, E. G. Birgin, and J. M. Martínez, "PACKMOL: A package for building initial configurations for molecular dynamics simulations," Journal of Computational Chemistry **30**, 2157–2164 (2009).
[68] B. Farkaš, U. Terranova, and N. H. d. Leeuw, "Binding modes of carboxylic acids on cobalt nanoparticles," Physical Chemistry Chemical Physics **22**, 985–996 (2020).